npj | Computational Materials

www.nature.com/npjcompumats

ARTICLE OPEN

Ferroelectric nonlinear anomalous Hall effect in few-layer WTe_2

Hua Wang[1] and Xiaofeng Qian[1*]

Under broken time reversal symmetry such as in the presence of external magnetic field or internal magnetization, a transverse voltage can be established in materials perpendicular to both longitudinal current and applied magnetic field, known as classical Hall effect. However, this symmetry constraint can be relaxed in the nonlinear regime, thereby enabling nonlinear anomalous Hall current in time-reversal invariant materials – an underexplored realm with exciting new opportunities beyond classical linear Hall effect. Here, using group theory and first-principles theory, we demonstrate a remarkable ferroelectric nonlinear anomalous Hall effect in time-reversal invariant few-layer WTe_2 where nonlinear anomalous Hall current switches in odd-layer WTe_2 except 1T′ monolayer while remaining invariant in even-layer WTe_2 upon ferroelectric transition. This even-odd oscillation of ferroelectric nonlinear anomalous Hall effect was found to originate from the absence and presence of Berry curvature dipole reversal and shift dipole reversal due to distinct ferroelectric transformation in even and odd-layer WTe_2. Our work not only treats Berry curvature dipole and shift dipole on an equal footing to account for intraband and interband contributions to nonlinear anomalous Hall effect, but also establishes Berry curvature dipole and shift dipole as new order parameters for noncentrosymmetric materials. The present findings suggest that ferroelectric metals and Weyl semimetals may offer unprecedented opportunities for the development of nonlinear quantum electronics.

npj Computational Materials (2019)5:119 ; https://doi.org/10.1038/s41524-019-0257-1

INTRODUCTION

In classical linear Hall effect, a transverse voltage can be developed in materials with broken time-reversal symmetry only (e.g. in the presence of external magnetic field or internal magnetization) due to Onsager's relation. Second and higher order conductivity tensors, however, are not subject to this constraint, thereby enabling nonlinear anomalous Hall effect (NAHE) in time-reversal invariant system.[1–4] NAHE was observed very recently in few-layer tungsten ditelluride (WTe_2),[5–11] a layered material which also holds rich physics including high-temperature quantum spin Hall phase[12–15] and electrostatic gating induced superconductivity[16,17] in its 1T′ monolayer and type-II Weyl semimetallicity,[18] large non-saturating magnetoresistance[19] and ultrafast symmetry switching[20] in its bulk phase.

Monolayer 1T′ WTe_2 is centrosymmetric with vanishing even-order nonlinear current response, however vertical electric field can break its two-fold screw rotation symmetry, generate Berry curvature dipole (BCD), and induce second-order nonlinear anomalous Hall current.[5–8] In contrast to monolayer WTe_2, bilayer WTe_2 is naturally noncentrosymmetric due to the loss of two-fold screw rotation symmetry, resulting in intrinsic nontrivial BCD in bilayer WTe_2.[9–11] Surprisingly, ferroelectric switching was recently discovered in semimetallic bilayer and few-layer WTe_2,[21] quite unusual as ferroelectricity and semimetallicity normally do not co-exist in the same material.[22] The subtlety lies in the reduced screening along the out-of-plane direction which gives rise to finite out-of-plane ferroelectric polarization while preserving in-plane semimetallic nature. Conductance hysteresis persisting up to 300 K shows its great potential for room temperature device application. These recent studies combined reveal a striking feature of noncentrosymmetric few-layer WTe_2 – the coexistence of ferroelectricity and NAHE within a single material, enkindling a few fundamentally and technologically important questions: what's the fundamental correspondence between NAHE and ferroelectricity in ferroelectric metals and Weyl semimetals? Compared to ferroelectric semiconductors,[23] what are the unique advantages of ferroelectric metals[21] and ferroelectric Weyl semimetals?[24,25]

Here using first-principles approach and group theoretical analysis we show an intriguing ferroelectric nonlinear anomalous Hall effect (FNAHE) in time-reversal invariant few-layer WTe_2. In particular, while both bilayer and trilayer WTe_2 possess switchable out-of-plane electric polarization, nonlinear transverse Hall current only switches in trilayer WTe_2 upon ferroelectric switching. The microscopic origin of FNAHE in trilayer WTe_2 is found to be rooted in the reversal of Berry curvature dipole and shift dipole upon ferroelectric transition, which reveals an exciting yet unexplored realm of ferroelectric metals and Weyl semimetals with potential applications in nonlinear electronics.

RESULTS AND DISCUSSION

Second-order dc current

Consider an oscillating electric field $\boldsymbol{E}(\boldsymbol{r},t)=\boldsymbol{E}(\omega)e^{i(\boldsymbol{k}\cdot\boldsymbol{r}-\omega t)}+\boldsymbol{E}(-\omega)e^{-i(\boldsymbol{k}\cdot\boldsymbol{r}-\omega t)}$ with $\boldsymbol{E}(\omega)=\boldsymbol{E}^{*}(-\omega)$ (e.g. under AC electric field or upon coherent light illumination), the second-order nonlinear dc current under minimal coupling approximation was derived by Sipe et al.[26], i.e., $j_a^0=\chi_{abc}(0;\omega,-\omega)E_b(\omega)E_c(-\omega)$, where χ_{abc} are the dc photocurrent susceptibility. In general j_a^0 consists of two parts depending on the polarization of electric field/incident light, including linear photogalvanic effect (LPGE) and circular photogalvanic effect (CPGE),[2,26,27] i.e., $j_a^0=j_a^L+j_a^C$. BCD-induced nonlinear photocurrent current was generalized to the multiple-band case by Morimoto et al.[28] using Floquet theory and Rostami et al.[29] using density matrix beyond semiclassical Boltzmann theory.

[1]Department of Materials Science and Engineering, Texas A&M University, College Station, TX 77843, USA. *email: feng@tamu.edu

Nonlinear photocurrent originating from CPGE is also known as injection current.[26]

Both LPGE and CPGE have intraband and interband contributions. For the sake of completeness we include all the terms as follows,

$$j_a^L = j_{a,\mathrm{intra}}^L + j_{a,\mathrm{inter}}^L \begin{cases} j_{a,\mathrm{intra}}^L = -2\frac{e^3}{\hbar^2}\mathrm{Re}\left(\frac{\tau}{1-i\omega\tau}\right)\epsilon_{adc}D_{bd}^{\mathrm{intra}}\mathrm{Re}(E_b(\omega)E_c(-\omega)) \\ j_{a,\mathrm{inter}}^L = -2\frac{e^3}{\hbar^2}\tau D_{a,bc}^{\mathrm{L,inter}}\mathrm{Re}(E_b(\omega)E_c(-\omega)) \end{cases} \quad (1)$$

$$j_a^C = j_{a,\mathrm{intra}}^C + j_{a,\mathrm{inter}}^C \begin{cases} j_{a,\mathrm{intra}}^C = -\frac{e^3}{\hbar^2}\mathrm{Im}\left(\frac{\tau}{1-i\omega\tau}\right)D_{ab}^{\mathrm{intra}}\mathrm{Im}(\boldsymbol{E}(\omega)\times\boldsymbol{E}(-\omega))_b \\ j_{a,\mathrm{inter}}^C = -\frac{e^3}{2\hbar^2}\tau D_{ab}^{\mathrm{C,inter}}\mathrm{Im}(\boldsymbol{E}(\omega)\times\boldsymbol{E}(-\omega))_b \end{cases} \quad (2)$$

Here τ is relaxation time and ϵ_{adc} is the Levi–Civita symbol. D_{ab}^{intra} is the well-known BCD for intraband nonlinear process.[2] $D_{ab}^{\mathrm{C,inter}}$ is BCD for interband process associated with CPGE.[9] $D_{a,bc}^{\mathrm{L,inter}}$ is shift dipole (SD), originated from the simultaneous displacement of wavepacket upon excitation. More specifically, they are given by

$$\begin{cases} D_{ab}^{\mathrm{intra}}(\mu) = \int_{BZ} f_0(\mu)\partial_a\Omega^b = \int_{BZ}[d\boldsymbol{k}]\sum_n f_n(\mu)v_n^a(\boldsymbol{k})\Omega_n^b(\boldsymbol{k})\delta(\hbar\omega_n(\boldsymbol{k})-\mu) \\ D_{ab}^{\mathrm{C,inter}}(\mu,\omega) = \int_{BZ}[d\boldsymbol{k}]\sum_{mn} f_{nm}(\mu)\Delta_{mn}^a(\boldsymbol{k})\Omega_{nm}^b(\boldsymbol{k})\mathrm{Re}\left(\frac{\tau}{1-i(\omega-\omega_{mn})\tau}\right) \\ D_{a,bc}^{\mathrm{L,inter}}(\mu,\omega) = \int_{BZ}[d\boldsymbol{k}]\sum_{mn} f_{nm}(\mu)R_{mn}^a(\boldsymbol{k})\{r_{nm}^b, r_{mn}^c\}\mathrm{Re}\left(\frac{1}{1-i(\omega-\omega_{mn})\tau}\right) \end{cases} \quad (3)$$

Here, $\hbar\omega_n(\boldsymbol{k})$, $v_n^b(\boldsymbol{k})$, and $f_n(\mu)$ are band energy, group velocity, and chemical-potential μ dependent Fermi-Dirac distribution, respectively. $f_{nm}(\mu) \equiv f_n(\mu) - f_m(\mu)$, and $[d\boldsymbol{k}] \equiv d^dk/(2\pi)^d$ for d-dimension integral. $\Delta_{nm}^a \equiv v_n^a - v_m^a$ is the group velocity difference between two bands. r_{nm}^a is interband Berry connection or dipole matrix element. $\Omega_{nm}^c(\boldsymbol{k})$ is the interband Berry curvature between two bands, defined as $\Omega_{nm}^c(\boldsymbol{k}) \equiv i\epsilon_{abc}r_{nm}^a r_{mn}^b$. $\Omega_n^c(\boldsymbol{k})$ is the intraband Berry curvature for band n, given by $\Omega_n^c(\boldsymbol{k}) = \sum_{n\neq m}\Omega_{mn}^c(\boldsymbol{k})$. In addition, $\{r_{nm}^b, r_{mn}^c\} \equiv r_{nm}^b r_{mn}^c + r_{mn}^c r_{nm}^b$. R_{mn}^a is shift vector, given by $R_{mn}^a \equiv -\frac{\partial\phi_{mn}(\boldsymbol{k})}{\partial k^a} + r_{mm}^a(\boldsymbol{k}) - r_{nn}^a(\boldsymbol{k})$, where $\phi_{mn}(\boldsymbol{k})$ is the phase factor of the interband Berry connection and r_{nn}^a is intraband Berry connection. $\Omega_{nm}^b(\boldsymbol{k})$, $\Omega_n^b(\boldsymbol{k})$ and R_{mn}^a are all gauge invariant. For linearly polarized incident light/electric field, $E_b = E_c$, hence we denote $D_{ab}^{\mathrm{L,inter}} \equiv D_{a,bc}^{\mathrm{L,inter}}$. The intraband and interband BCDs (D_{ab}^{intra}, $D_{ab}^{\mathrm{C,inter}}$) as well as SD ($D_{ab}^{\mathrm{L,inter}}$) have the same units of L^{3-d} for d-dimensional system. Thus, BCD and SD have units of length in 2D, but become dimensionless in 3D.

The appearance of relaxation time τ in the dc current from interband LPGE ($j_{a,\mathrm{inter}}^L$) seems different from the widely-used τ-independent shift current formula by Sipe et al.[26], however the latter was derived for the clean limit when relaxation time τ approaches to infinite. In fact, as $\tau\to\infty$, $\tau\mathrm{Re}\left(\frac{1}{1-i(\omega-\omega_{mn})\tau}\right) \to \pi\delta(\omega_{mn}-\omega)$, and the original τ-time independent shift current susceptibility can be exactly recovered from the above $j_{a,\mathrm{inter}}^L$ formula. In reality, quasiparticles do have finite relaxation time, thus $j_{a,\mathrm{inter}}^L$ shall depend on relaxation time. More detailed derivation about the SD and BCD can be found in the Supplementary Information.

Moreover, it is worth to classify the contributions of LPGE/CPGE-induced dc current at the low/high frequency region. At the low frequency limit, $\omega\tau\to 0$, hence $\frac{\tau}{1-i\omega\tau}\to\tau$. In this case, the photocurrent due to both intraband and interband CPGE as well as interband LPGE will vanish, however a dc current from intraband LPGE will remain finite which is perpendicular to the applied electric field, thereby inducing *static* NAHE. At high frequency, CPGE (*i.e.* injection current) and interband LPGE (*i.e.* shift current) will have nontrivial contribution to total nonlinear photocurrent, referred as to *dynamic* NAHE.

It is important to note that the direction of nonlinear photocurrent induced by CPGE and LPGE have very different symmetry properties. The LPGE-induced dc current cannot flow normal to a mirror plane, however it is allowed for the CPGE-induced dc current. This distinct symmetric property of CPGE- and LPGE-induced dc current can be used to help distinguish different contributions. In fact, this is what we will see in bilayer and trilayer WTe_2.

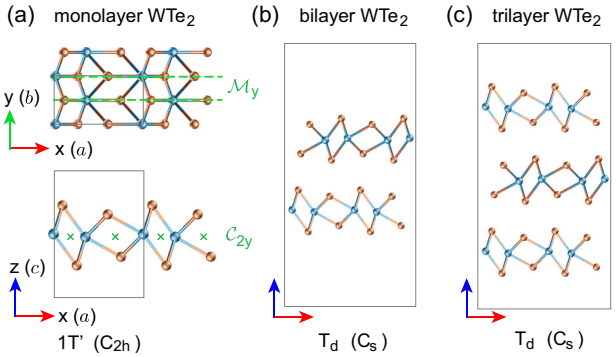

Fig. 1 Crystal structure of monolayer, bilayer, and trilayer WTe_2. **a** Monolayer 1T′ WTe_2 with centrosymmetric C_{2h} point group. It has a mirror plane $\mathcal{M}_y$ and a screw rotation symmetry C_{2y}, which leads to the inversion symmetry $\mathcal{I} = \mathcal{M}_y C_{2y}$. **b, c** Bilayer and trilayer T_d WTe_2 with C_s point group. C_{2y} symmetry is broken, hence the inversion symmetry $\mathcal{I}$ is also broken in bilayer and trilayer WTe_2.

More importantly, nonlinear dc current may switch their direction upon certain ferroelectric transition, giving rise to *FNAHE* which is the focus of this work. Below we will first reveal the fundamental difference between ferroelectric transitions in bilayer and trilayer WTe_2, then demonstrate a striking even-odd anomaly of NAHE, *i.e. FNAHE*, in bilayer and trilayer WTe_2 and provide an explanation using group theoretical analysis as well as its implication for potential FNAHE-based quantum devices.

Ferroelectric transition in bilayer and trilayer WTe_2

Both bilayer and trilayer WTe_2 were found to exhibit ferroelectric switching, however their transformation is fundamentally different, which plays a key role in their distinct NAHE. Crystal structures of monolayer, bilayer, and trilayer WTe_2 are shown in Fig. 1. Monolayer 1T′ WTe_2 has a C_{2h} point group with a mirror plane symmetry $\mathcal{M}_y$ perpendicular to y-axis and a two-fold screw rotation symmetry C_{2y}. This leads to inversion symmetry $\mathcal{I} = \mathcal{M}_y C_{2y}$ or $C_{2y}\mathcal{M}_y$. Upon van der Waals (vdW) T_d stacking, multilayer noncentrosymmetric T_d WTe_2 possesses mirror plane symmetry $\mathcal{M}_y$ only, and no longer holds C_{2y} symmetry as the rotation axes of different layers are not related by any symmetry operation in the point group. Consequently, multilayer T_d WTe_2 loses inversion center with C_s point group.

Ferroelectric transition pathways of bilayer and trilayer T_d WTe_2 are shown in Fig. 2. In both cases, two opposite ferroelectric (FE) states (Fig. 2a, c for bilayer, Fig. 2d, f for trilayer) can switch to each other by a small in-plane shift between adjacent layers along x by $2d_x$ ($d_x \sim 20$pm), passing through an intermediate paraelectric (PE) state. The intermediate PE state in bilayer WTe_2 (Fig. 2b) has a C_{2v} point group with additional $\left\{\mathcal{M}_z|\frac{1}{2}a\right\}$ symmetry, thus its out-of-plane electric polarization P_z vanishes. While the ferroelectric transition is achieved by in-plane $2d_x$ shift, two FE states are related by a glide plane operation $\{\mathcal{M}_z|t_a\}$ consisting of a mirror symmetry operation followed by a translation along x by a fractional translation t_a where $t_a = \frac{1}{2}a$. For this reason, we denote the two FE states of bilayer WTe_2 by $-m$FE and $+m$FE (Fig. 2a, c). In contrast, the two opposite FE states in trilayer WTe_2 are related by an inversion operation $\mathcal{I}$, denoted by $-i$FE and $+i$FE (Fig. 2d, f). Furthermore, its intermediate PE state has a C_{2h} point group with

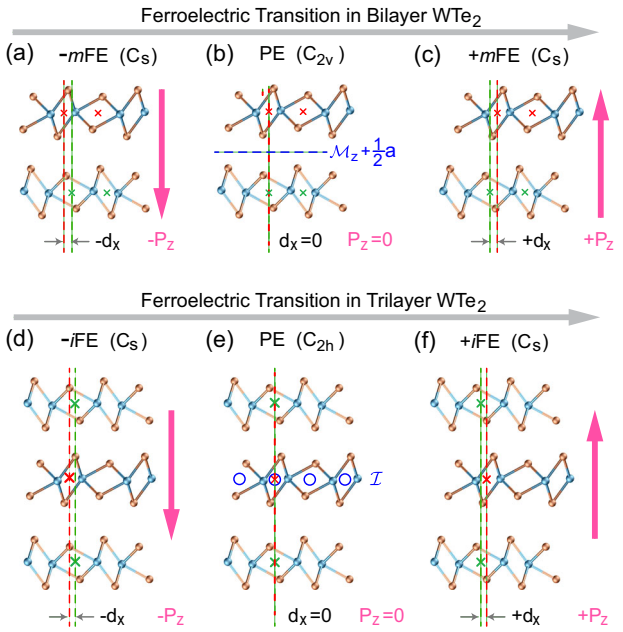

Fig. 2 Ferroelectric transition in bilayer and trilayer WTe_2. a–c ferroelectric transition in bilayer WTe_2. The two opposite ferroelectric states ($-m$FE and $+m$FE) in bilayer are transformed through a glide plane operation $\{\mathcal{M}_z|t_a\}$, that is, a mirror operation $\mathcal{M}_z$ followed by an in-plane shift along x by t_a with $t_a = \frac{1}{2}a$. The intermediate PE state C_{2v} point group, thus its out-of-plane polarization with vanishes due to the glide plane $\{\mathcal{M}_z|\frac{1}{2}a\}$ symmetry. **d–f** ferroelectric transition in trilayer WTe_2. The two opposite ferroelectric states ($-i$FE and $+i$FE) in trilayer are related to each other through an inversion operation $\{\mathcal{I}|0\}$. The intermediate PE state of trilayer WTe_2 has C_{2h} point group, thus its out-of-plane polarization also vanishes due to inversion symmetry. The red and green vertical dashed lines show the relative shift $\pm d_x$ between adjacent WTe_2 layers. The corresponding in-plane shift is very small ($d_x \approx 20$ pm), therefore it is exaggerated in the above plots for illustrative purpose.

inversion symmetry, hence the out-of-plane polarization P_z of the PE state in trilayer WTe_2 vanishes as well.

Next, we calculate total electric polarization by summing the ionic and electronic contributions. Since we are interested in the polarization along the out of plane direction P_z, we can directly integrate the product between charge density/ionic charge and their corresponding position to obtain P_z without using Berry phase approach. More specifically, $P_z = \frac{1}{S}\left(\sum_I Q_I \cdot \left(z_I - \boldsymbol{R}_0^z\right) - e\int_V \rho(\boldsymbol{r})\left(z - \boldsymbol{R}_0^z\right)d^3r\right)$, where S is the in-plane area of the unit cell, Q is ionic charge, ρ is electronic charge density, and $\boldsymbol{R}_0$ is a reference point which is set to the origin of the unit cell in the present case. The equilibrium electronic charge density $\rho(\boldsymbol{r})$ was obtained from first-principles density functional theory (DFT)[30,31] as implemented in the Vienna Ab initio Simulation Package (VASP).[32] The calculated total electric polarization P_z is $\pm 1.67 \times 10^{-2}$ nm μC/cm^2 for $\pm m$FE in bilayer, and $\pm 0.81 \times 10^{-2}$ nm μC/cm^2 for $\pm i$FE in trilayer. This is in good agreement with experimentally measured vertical polarization in bilayer WTe_2 of $\sim 10^4$ e cm^{-1} (i.e. 1.60×10^{-2} nm μC/cm^2).[21] Additionally, the intermediate PE state was recently observed in experiments.[20] In brief, the results from the DFT calculations confirmed the ferroelectricity in both bilayer and trilayer WTe_2, however the symmetry relations between the two FE states are very different in the bilayer and trilayer cases, *i.e.* $-m$FE ↔ PE ↔ $+m$FE and $-i$FE ↔ PE ↔ $+i$FE, which is essential for understanding their distinct NAHE upon ferroelectric switching we will discuss shortly.

NAHE in bilayer and trilayer WTe_2 upon ferroelectric switching

Now we proceed to discuss NAHE in few-layer WTe_2, in particular ferroelectric switching of NAHE (*i.e.* FNAHE) in odd-layer WTe_2, and reveal the intriguing connection between BCD/SD and ferroelectric order. We compute their electronic structure by first-principles DFT using hybrid exchange-correlation functional with spin-orbit coupling taken into account. Quasiatomic spinor Wannier functions and tight-binding Hamiltonian were obtained by rotating and optimizing the Bloch functions with a maximal similarity measure with respect to pseudoatomic orbitals.[33,34] Subsequently, first-principles tight-binding approach was applied to compute all the physical quantities such as band structure, BCD, SD, Berry curvature etc. More calculation details can also be found in Methods Section.

Electronic band structure of bilayer WTe_2 is presented in Fig. 3a, color-coded by total intraband Berry curvature of all occupied bands, that is, $\Omega^{z,\mathrm{intra}}_{\mathrm{occ}}(\boldsymbol{k}) = \sum f_n \Omega^z_n(\boldsymbol{k})$. It shows bilayer WTe_2 is a small gap insulator, and the intraband Berry curvature is odd with respect to Γ due to the presence of time-reversal symmetry. The $\boldsymbol{k}$-dependent intraband Berry curvature $\Omega^{z,\mathrm{intra}}_{\mathrm{occ}}(\boldsymbol{k})$ are shown in Fig. 3c, d at two different chemical potentials of $\mu = \pm 50$ meV. Alternatively, one may use the Kubo formula with the sum-over-states approach for Berry curvature (see Supplementary Fig. 2). Similarly, interband Berry curvature $\Omega^z_{nm}(\boldsymbol{k})$ with at frequency $\omega =$ 120 meV is displayed in Fig. 3e, f for two sets of occupied and unoccupied bands around the Fermi energy, $\Omega^{z,\mathrm{inter}}_{\mathrm{VBM}-1,\mathrm{CBM}}(\boldsymbol{k})$ and $\Omega^{z,\mathrm{inter}}_{\mathrm{VBM,CBM}-1}(\boldsymbol{k})$, respectively. VBM refers to valence band maximum, and CBM refers to conduction band minimum. The Berry curvature distribution plots confirm the presence of mirror symmetry $\mathcal{M}_y$ and time-reversal symmetry $\mathcal{T}$. Thus, the integral of the intraband Berry curvature over the full Brillouin zone vanishes, and linear anomalous Hall effect is absent. Furthermore, Fig. 3b shows the calculated BCD and SD tensor elements – D^{intra}_{yz}, $D^{\mathrm{C,inter}}_{yz}$, and $D^{\mathrm{L,inter}}_{xy}$ – the key physical quantities governing NAHE. It clearly demonstrates the presence of finite BCD and SD and thus NAHE in bilayer WTe_2. The calculated BCD varies between 0 and 0.4 Å depending on the chemical potential, which is in nice agreement with the experimental values of 0.1–0.7 Å by Kang et al.[10]. Moreover, upon ferroelectric transition between $-m$FE and $+m$FE state, the Berry curvature, BCD and SD remain unchanged, thus nonlinear anomalous Hall current will not switch direction upon ferroelectric transition in bilayer WTe_2. Similarly, the out-of-plane spin polarization remains unflipped, while the in-plane spin polarization is expected to reverse (see Supplementary Figs. 3 and 4). Furthermore, Du et al. recently studied NAHE in bilayer WTe_2 using a model Hamiltonian and found that, as the SOC strength evolves, BCD becomes strong near tilted band anticrossings and band inversions.[11] Our first-principles results also show large Berry curvature near band anticrossings which is consistent with the conclusion from Du et al.'s analysis. The magnitude of the calculated Berry curvature is similar to that in Ma et al.[9] for bilayer WTe_2 in the absence of electric field. The difference in the detailed band structure is mainly due to the electronic structure sensitive to DFT exchange-correlation functional, vdW functional, and the Wannier function construction. Nevertheless, both our results and the work by Ma et al.[9] show the nontrivial BCD contribution to NAHE.

Trilayer WTe_2 is quite different from bilayer WTe_2. Figure 4a, b show its electronic band structure of $-i$FE and $+i$FE state, respectively. In contrast to the bilayer case, intraband Berry curvature changes sign upon ferroelectric transition. The similar sign change is also evidenced in the opposite $\boldsymbol{k}$-dependent intraband and interband Berry curvature $\Omega^{z,\mathrm{intra}}_{\mathrm{occ}}(\boldsymbol{k})$ and $\Omega^{z,\mathrm{inter}}_{\mathrm{VBM}-1,\mathrm{CBM}}(\boldsymbol{k})$ as displayed in Fig. 4e–h. Consequently, the sign of BCD and SD flips upon ferroelectric transition between $-i$FE and $+i$FE, demonstrated in Fig. 4c, d. Therefore, in direct contrast to bilayer WTe_2, the nonlinear dc current in trilayer WTe_2 will

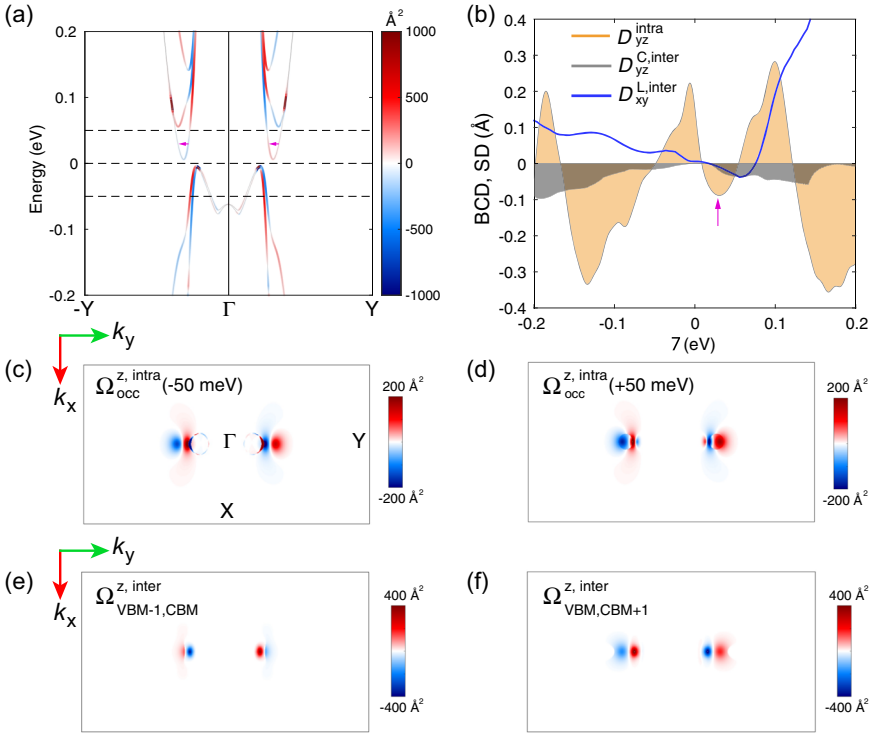

Fig. 3 Electronic structure and NAHE of bilayer WTe_2. a Band structure of bilayer WTe_2 in ±*m*FE state color-coded by the z-component of intraband Berry curvature $\Omega_n^z(\boldsymbol{k})$. Spin-orbit coupling is included and hybrid HSE06 functional is employed. **b** BCD and SD tensor elements $D_{yz}^{intra}(\mu)$, $D_{yz}^{C,inter}(\mu,\omega)$, and $D_{xy}^{L,inter}(\mu,\omega)$ as function of chemical potential μ. For interband BCD and SD, ω is set to 120 meV**. c**, **d** ***k***-dependent distribution of intraband Berry curvature $\Omega_{occ}^{z,intra}(\boldsymbol{k})$ at $\mu = \pm 50$ meV, respectively. **e**, **f** ***k***-dependent distribution interband Berry curvature $\Omega_{nm}^{z,inter}(\boldsymbol{k})$ for $(n, m) =$ (VBM-1, CBM) and for $(n, m) =$ (VBM-1,CBM), respectively. The results are the same for both +*m*FE and −*m*FE state, suggesting that nonlinear anomalous Hall current can be induced in bilayer WTe_2, but it will not switch sign upon ferroelectric transition.

switch its direction upon ferroelectric transition. The calculated BCD ranges from 0 to 0.7 Å depending on the chemical potential, also in good agreement with experiment.[10] Moreover, there is a clear plateau in $D_{yz}^{C,inter}$ marked by purple arrow in Fig. 4c. It is originated from the large joint density of state around 120 meV indicated by purple arrow in Fig. 4a, which remains constant when the chemical potential is located between the energy window. It is also worth to note that, like the bilayer case, the integral of Berry curvature of trilayer WTe_2 is also zero due to the presence of time-reversal symmetry, hence the linear anomalous Hall effect is absent. Both in-plane and out-of-plane spin polarizations are reversed (see Supplementary Figs. 5 and 6). Finally, the dc current susceptibility of bilayer and trilayer WTe_2 will be reversed in the trilayer case only. Figure 5 shows the interband LPGE susceptibility σ_{abc} of bilayer and trilayer WTe_2 at $\mu = 0$, which is about 10 times higher than that in monolayer group IV monochalcogenides.[23] It is clear that in bilayer WTe_2 the two independent susceptibility tensor elements σ_{xxx} and σ_{xyy} of the ±*m*FE states remain invariant upon ferroelectric transition, while for trilayer WTe_2 both σ_{xxx} and σ_{xyy} of the ±*i*FE states flip the sign.

The above electronic structure results demonstrate a striking difference between bilayer and trilayer WTe_2, that is, nonlinear anomalous Hall current flips its direction upon ferroelectric switching in trilayer WTe_2, but remains unchanged in bilayer WTe_2.

Group theoretical analysis of NAHE in bilayer and FNAHE in trilayer WTe_2

Here we provide a group theoretical analysis of NAHE in addition to the above first-principles calculations. Both bilayer and trilayer WTe_2 have C_s point group with a mirror symmetry M_y. For circularly polarized incident light propagating along z, $(\boldsymbol{E}(\omega) \times \boldsymbol{E}(-\boldsymbol{\omega}))_z$, shares the same A'' representation as axial vector R_z. Therefore, $\Gamma_{j_y} \otimes \Gamma_{\boldsymbol{R_{xz}}} = A'' \otimes A'' = A'$, suggesting $\Gamma_{j_y} \otimes \Gamma_{\boldsymbol{R_{xz}}}$ includes total symmetric irreducible representation, and hence nonlinear CPGE current can be induced along *y*, i.e., perpendicular to the *xz* mirror plane. Furthermore, $\Gamma_{j_{xz}} \otimes \Gamma_{\boldsymbol{R_{xz}}} = A''$, thus no CPGE current can be induced along *x*. In contrast, for linearly polarized incident light/electric field with in-plane polarization, we have $\Gamma_{j_x} \otimes \Gamma_{E_x} \otimes \Gamma_{E_x} = A' \otimes A' \otimes A' = A'$, and $\Gamma_{j_x} \otimes \Gamma_{E_y} \otimes \Gamma_{E_y} = A' \otimes A'' \otimes A'' = A'$, indicating that the LPGE current can be induced along *x*. However, $\Gamma_{j_y} \otimes \Gamma_{E_x} \otimes \Gamma_{E_x} = \Gamma_{j_y} \otimes \Gamma_{E_y} \otimes \Gamma_{E_y} = A''$, thus no LPGE current can be induced along *y*. This leads to a contrasting CPGE- and LPGE-based nonlinear anomalous Hall current in few-layer WTe_2 with C_s point group, that is, linearly polarized light/electric field with in-plane polarization will generate nonlinear anomalous Hall current along *x* only $(j_x^L \neq 0, j_y^L = 0)$, while circularly polarized light propagating along *z* axis will generate nonlinear anomalous Hall current along *y* only $(j_x^C = 0, j_y^C \neq 0)$.

The correlation between the irreducible representations of parent group C_{2h} and its noncentrosymmetric subgroups C_2, C_s, and C_1 is summarized in Supplementary Table 1. We start from monolayer 1T′ WTe_2 which has point group of C_{2h}, whose second order nonlinear current response vanishes due to the presence of inversion symmetry. Upon vdW stacking (e.g. few-layer and bulk T_d WTe_2), C_{2y} is broken with M_y left unchanged, which breaks the inversion symmetry and results in subgroup C_s. Consequently, as we analyzed above, $j_x^C = 0$, but $j_y^C \neq 0$ under circularly polarized light, while $j_x^L \neq 0$ but $j_y^L = 0$ under linearly polarized light/electric field with in-plane polarization. However, if M_y is broken with C_{2y} being preserved, it will fall into subgroup C_2. In this case, $j_x^C \neq 0$ and $j_y^C = 0$ under circularly polarized light, while $j_x^C = 0$ and $j_y^C \neq 0$ under linearly x/y-polarized light/electric field. Furthermore, if

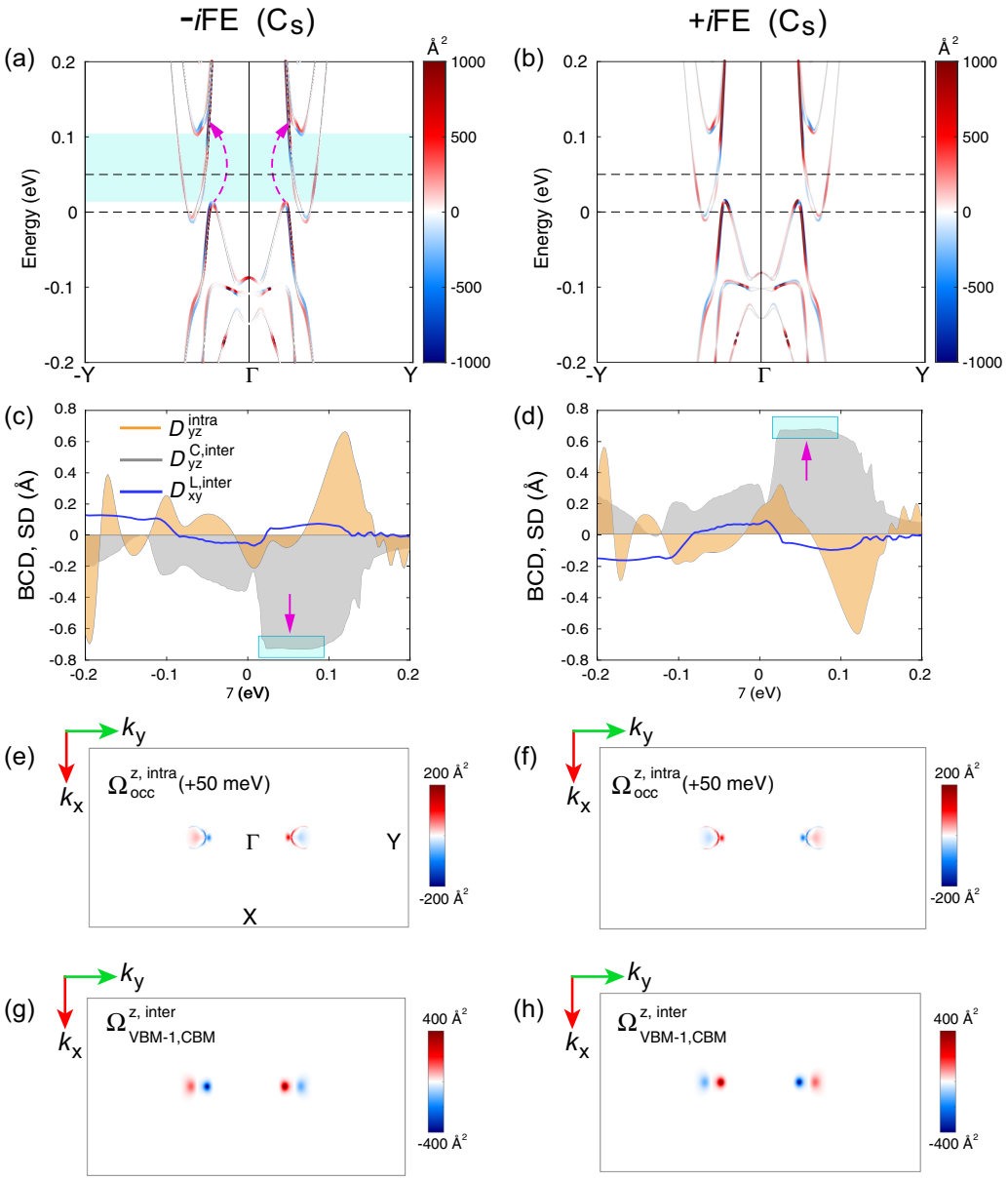

Fig. 4 Electronic structure and FNAHE of trilayer WTe_2. a, b Band structure of trilayer WTe_2 in $-i$FE and $+i$FE state, respectively. Both are color-coded by the z-component of intraband Berry curvature $\Omega_n^z(\boldsymbol{k})$. **c, d** BCD tensor elements $D_{yz}^{intra}(\mu)$ and $D_{yz}^{C,inter}(\mu,\omega)$, and SD tensor element $D_{xy}^{L,inter}(\mu,\omega)$ as function of chemical potential μ for $-i$FE and $+i$FE state, respectively. For interband BCD and SD, ω is set to 120 meV. **e, f** $\boldsymbol{k}$-dependent distribution of intraband Berry curvature $\Omega_{occ}^{z,intra}(\boldsymbol{k})$ at $\mu = \pm 50$ meV for $-i$FE and $+i$FE state, respectively. **g, h** $\boldsymbol{k}$-dependent distribution interband Berry curvature $\Omega_{nm}^{z,inter}(\boldsymbol{k})$ between (VBM-1,CBM) around the Fermi surface for $-i$FE and $+i$FE state, respectively. The results clearly show that nonlinear anomalous Hall current in trilayer WTe_2 will switch sign upon ferroelectric transition, in direct contrast to the bilayer case.

both M_y and C_{2y} are broken, it will end up with subgroup C_1, and enable all possible LPGE and CPGE current responses along different directions.

We now discuss the fundamental difference of NAHE between bilayer and trilayer WTe_2 upon ferroelectric switching. A general symmetry operator in Seitz notation is given by $g = \{R|\boldsymbol{t}_R\}$, where R is point group symmetry operation and $\boldsymbol{t}_R$ is a translational vector. A time-reversal antisymmetric pseudovector (e.g. Berry curvature and spin polarization) transforms under operator g as follows, $\boldsymbol{m}'(\boldsymbol{k}) = g\boldsymbol{m}(\boldsymbol{k}) = P_R P_T R\boldsymbol{m}(\boldsymbol{k})$, where P_R and P_T are spatial and temporal parity associated with g, respectively. $P_T = \pm 1$ when $R\boldsymbol{k} = \pm\boldsymbol{k} + \boldsymbol{K}$, where $\boldsymbol{K}$ is multiples of reciprocal lattice vector. For bilayer WTe_2, as aforementioned, two ferroelectric states can be related by a glide plane operation $\{\mathcal{M}_z|t_a\}$, where t_a refers to a fractional translation along x. Thus, $P_R = -1$, $P_T = 1$, and $(m_x, m_y, m_z)^{+mFE} = (-m_x, -m_y, m_z)^{-mFE}$. For trilayer WTe_2, the two ferroelectric states are related by an inversion operation $\{\mathcal{I}|0\}$, thus $P_R = P_T = -1$, subsequently $(m_x, m_y, m_z)^{+iFE} = (-m_x, -m_y, -m_z)^{-iFE}$. The above two conclusions are applicable to any time-reversal antisymmetric pseudovectors such as Berry curvature and spin polarization. For example, for intraband and interband Berry curvature, $\mathcal{M}_z\Omega^z(k_x,k_y) = \Omega^z(k_x,k_y)$ in bilayer WTe_2, and $\mathcal{I}\Omega^z(k_x,k_y) = \Omega^z(-k_x,-k_y) \xrightarrow{TRI} -\Omega^z(k_x,k_y)$ in trilayer WTe_2, indicating that the sign of intraband and interband BCD (D_{ab}^{intra}, $D_{ab}^{C,inter}$) flips only in trilayer WTe_2 upon ferroelectric transition. This is in

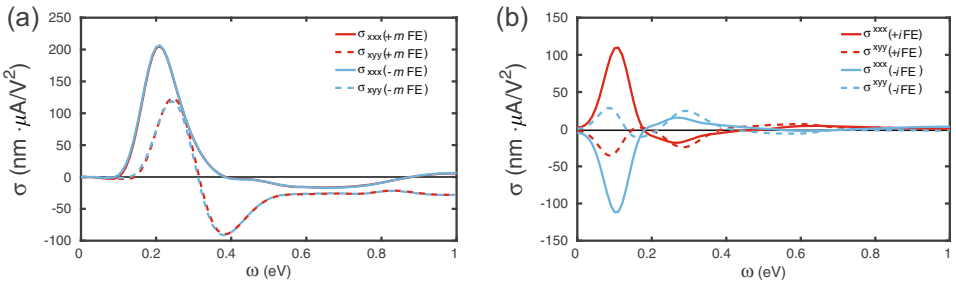

Fig. 5 Interband LPGE susceptibility σ_{abc} of bilayer and trilayer WTe_2 at $\mu = 0$. a σ_{abc} for the $\pm m$FE states of bilayer WTe_2. **b** σ_{abc} for the $\pm i$FE state of trilayer WTe_2. These two plots demonstrate that, under ferroelectric transition, the sign of LPGE-induced dc current susceptibility switches in the trilayer case, but remains invariant in the bilayer case.

excellent agreement with the first-principles calculations shown in Fig. 3c–f and Fig. 4e–h. In addition, the in-plane spin polarization switches in both cases, and the out-of-plane spin polarization becomes reversed in trilayer WTe_2 while remaining unflipped for bilayer WTe_2, which also agrees with the calculations (Supplementary Figs. 3–6). Different from pseudovectors, polar vector $\boldsymbol{p}$ such as electric polarization and shift vector transforms as follows: $\boldsymbol{p}' = R\boldsymbol{p}$ Therefore, both mirror $\mathcal{M}_z$ and inversion $\mathcal{I}$ operation will lead to vertical polarization reversal, *i.e.* $p'_z = \mathcal{M}_z p_z = -p_z$ and $p'_z = \mathcal{I} p_z = -p_z$, *i.e.* the out-of-plane electric dipole flips sign in both bilayer and trilayer WTe_2 upon ferroelectric transition. In addition, for in-plane shift vector R^a_{mn} with $a \in \{x, y\}$, $(R^a_{mn})' = \mathcal{M}_z R^a_{mn} = R^a_{mn}$, and $(R^a_{mn})' = \mathcal{I} R^a_{mn} = -R^a_{mn}$, indicating that the in-plane shift vector R^a_{mn} and thus SD $D^{\text{L,inter}}_{yz}$ will flip only in trilayer WTe_2 upon ferroelectric transition. Consequently, the total j^L_x and j^C_y from CPGE and LPGE will switch direction upon ferroelectric transition, provoking FNAHE in time-reversal invariant semimetals. Moreover, it suggests that the BCD and SD can serve as distinct order parameters for noncentrosymmetric semimetals. Figure 6a presents an illustrative summary of the transformation of Berry curvature, spin polarization, and electric polarization under different symmetry operation, while Fig. 6b, c show the ferroelectric switching of nonlinear current in the $-i$FE and $+i$FE state of trilayer WTe_2. Upon the out-of-plane polarization switching, nonlinear Hall current j^L_x generated via LPGE switches between $-x$ and $+x$ direction under the same external electric field with in-plane linear polarization. Moreover, nonlinear Hall current j^C_x induced by CPGE switches between $-y$ and $+y$ direction under circularly-polarized light with normal incidence. It's worth to emphasize that the intermediate PE state in bilayer and trilayer WTe_2 has noncentrosymmetric C_{2v} and centrosymmetric C_{2h} point group, respectively. Thus, despite that the out-of-plane electric polarization vanishes in both cases, nonlinear anomalous Hall current of the PE state vanishes in trilayer, but remains finite in bilayer.

The present work considers intrinsic NAHE due to BCD. Disorder however can play an important role in NAHE as pointed out by Du et al.[35] and Isobe et al.[36] particularly in the dc limit due to side jump and skew scattering.[37] As disorder scattering depends on scattering potential and defect density, further experimental studies are required to understand the nature of defects in bilayer and trilayer WTe_2. The transformation behavior of BCD-induced NAHE in multilayer WTe_2 upon ferroelectric transition may be utilized to distinguish itself from the disorder scattering-induced NAHE. For example, upon ferroelectric transition, the change in defect scattering potential may behave very differently from the change in crystal structure, thereby potentially helping differentiate the two NAHE contributions.

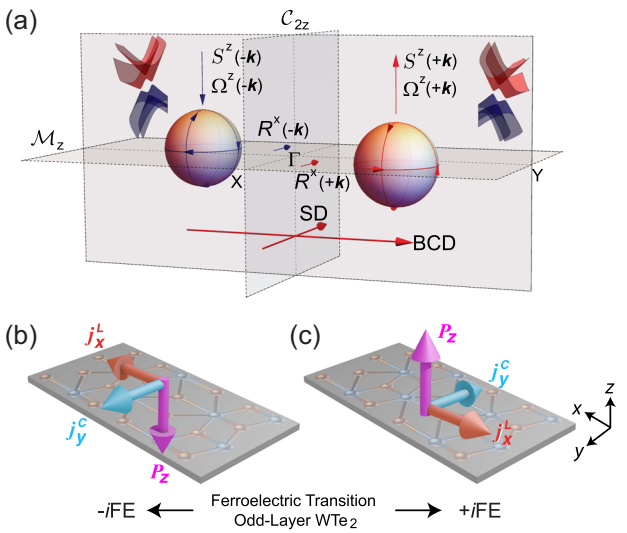

Fig. 6 Transformation of pseudovectors and polar vectors under different symmetry operation and ferroelectric switching of LPGE and CPGE nonlinear current. a Transformation of Berry curvature, spin polarization, shift vector, BCD and SD as well as LPGE and CPGE nonlinear current under different symmetry operation between two ferroelectric states in time-reversal invariant few-layer WTe_2. Berry curvature and spin polarization transform as time-reversal antisymmetric pseudovectors. Under a mirror symmetry operation $\mathcal{M}_z$ for the ferroelectric states in bilayer WTe_2, most quantities remain invariant, except in-plane spin and Berry curvature component. Under inversion symmetry operation $\mathcal{I}$ for the $-i$FE and $+i$FE state states in trilayer WTe_2, all quantities, including Berry curvature, spin polarization, shift vector, BCD and SD, flip the sign in the presence of time-reversal symmetry, giving rise to FNAHE in trilayer WTe_2. **b**, **c** Ferroelectric switching of nonlinear current in the $-i$FE and $+i$FE state of trilayer WTe_2, respectively. Upon the polarization P_z switching, nonlinear anomalous Hall current j^L_x from LPGE switches between $-x$ and $+x$ direction under external field with in-plane linear polarization, while nonlinear anomalous Hall current j^C_y from CPGE switches between $-y$ and $+y$ direction under circularly-polarized light with normal incidence.

In conclusion, using first-principles calculations and group theoretical analyses we investigated the NAHE in bilayer and trilayer WTe_2 and, more importantly, the underlying microscopic origin of FNAHE (i.e., ferroelectric switching of NAHE) in trilayer WTe_2. Although both bilayer and trilayer WTe_2 exhibit ferroelectric transition with similar electric polarization, they behave very differently in NAHE. In the trilayer case, the nonlinear anomalous Hall current flips direction upon ferroelectric switching due to the reversal of BCD and SD under an effective inversion operation of the two ferroelectric states. In contrast, the two ferroelectric states

in bilayer WTe_2 are related effectively by a glide plane operation which does not flip the BCD/SD, thus its nonlinear anomalous Hall current will not flip upon ferroelectric switching. In addition, NAHE is expected to vanish in the PE state of trilayer WTe_2, but remains nontrivial for the PE state of the bilayer case. The above conclusions are applicable to any even and odd layer WTe_2 (except monolayer 1T′ WTe_2 as it is centrosymmetric with vanishing second order NAHE) as long as the two opposite ferroelectric states have the same relationship as the bilayer and trilayer case. The theoretical approaches presented here can also be applied to other materials such as Weyl semimetals.[24,25]

More importantly, our results imply that BCD and SD can serve as new order parameters for noncentrosymmetric materials, which opens up the possibility to explore nonlinear multiferroicity based on the coupling of BCD/SD and ferroelectric order. Ferroelectric metals may be advantageous as their vanishing bandgap will not only bring intraband contributions to nonlinear anomalous Hall current that is absent in semiconductors/insulators, but also significantly enhance the interband contributions due to the reduced gap of nonlinear interband processes. For example, the calculated nonlinear anomalous Hall current from interband LPGE in bilayer and trilayer WTe_2 is about one order of magnitude higher than that in ferroelectric GeS.[23] Moreover, FNAHE provides a facile approach for direct readout of ferroelectric states, which, combined with vertical ferroelectric writing, may allow for realizing nonlinear multiferroic memory. In addition, the distinct ferroelectric transformation pathway may provide potential routes to realizing non-abelian reciprocal braiding of Weyl nodes.[38] The present findings therefore reveal an underexplored realm beyond classical linear Hall effect and conventional ferroelectrics with exciting new opportunities for FNAHE-based nonlinear quantum electronics using ferroelectric metals and Weyl semimetals.

METHODS

First-principles calculations of atomistic and electronic structure

First-principles calculations for structural relaxation and electric polarization were performed using density-functional theory[30,31] as implemented in the Vienna Ab initio Simulation Package (VASP)[32] with the projector-augmented wave method.[39] We employed the generalized-gradient approximation of exchange-correlation functional in the Perdew–Burke–Ernzerhof form,[40] a plane-wave basis with an energy cutoff of 300 eV, a Monkhorst–Pack k-point sampling of $6 \times 12 \times 1$ for the Brillouin zone integration, and optB88-vdW functional[41] to account for dispersion interactions. Ground state crystal structures were obtained by fully relaxing both atomic positions and in-plane lattice parameters while keeping a large vacuum region of ~20 Å along the out-of-plane direction to reduce the periodic image interactions. The convergence criteria for maximal residual force was <0.005 eV/Å, and the convergence criteria for electronic relaxation is 10^{-6} eV. We have tested higher energy cutoff of 400 eV, and the difference in the lattice constants is <0.04%. Crystal structures of bilayer and trilayer WTe_2 can be found in the Supplementary Information. In addition, total electric polarization was calculated by directly integrating the product of charge density/ionic charge and their corresponding position without using Berry phase approach.

First-principles electronic structure calculations of NAHE

To compute the NHLE-related quantities, we first construct quasiatomic spinor Wannier functions and tight-binding Hamiltonian from Kohn–Sham wavefunctions and eigenvalues under the maximal similarity measure with respect to pseudoatomic orbitals.[33,34] Spin-orbit coupling is taken into account, and hybrid exchange-correlation energy functional HSE06[42] is employed with the range-separation parameter $\lambda = 0.2$ (see Supplementary Information for more details). Total 112 and 168 quasiatomic spinor Wannier functions were obtained for bilayer and trilayer WTe_2, respectively. Using the developed tight-binding Hamiltonian we then compute CPGE and LPGE susceptibility tensor with a modified WANNIER90 code[43] using a dense k-point sampling of $600 \times 600 \times 1$ for both bilayer and trilayer WTe_2. A small imaginary smearing factor η of 0.05 eV is applied to fundamental frequency, and Sokhotski–Plemelj theorem is employed for the Dirac delta function integration. In addition, we tested the range separation parameter λ in the hybrid HSE functional. Although the values of Berry curvature etc. can change with respect to λ, the presence (absence) of Berry curvature switching in trilayer (bilayer) remains the same (see Supplementary Fig. 3 for HSE functional with $\lambda = 0.4$). We also checked the convergence of the k-point sampling by increasing it to $1000 \times 1000 \times 1$ (Supplementary Fig. 7). Finally, since few-layer WTe_2 is either semimetallic or having very small gap, the dielectric screening is large, thus the effect of the Coulombic interaction between electrons and holes is negligible.

DATA AVAILABILITY

The datasets generated during and/or analyzed during the current study are available from the corresponding author upon reasonable request.

Received: 22 August 2019; Accepted: 12 November 2019;
Published online: 06 December 2019

REFERENCES

1. Moore, J. E. & Orenstein, J. Confinement-induced berry phase and helicity-dependent photocurrents. *Phys. Rev. Lett.* **105**, 026805 (2010).
2. Sodemann, I. & Fu, L. Quantum Nonlinear Hall effect induced by berry curvature dipole in time-reversal invariant materials. *Phys. Rev. Lett.* **115**, 216806 (2015).
3. Low, T., Jiang, Y. & Guinea, F. Topological currents in black phosphorus with broken inversion symmetry. *Phys. Rev. B* **92**, 235447 (2015).
4. Deyo, E., Golub, L., Ivchenko, E. & Spivak, B. Semiclassical theory of the photogalvanic effect in non-centrosymmetric systems. *Preprint at arXiv:0904.1917* (2009).
5. Xu, S.-Y. et al. Electrically switchable Berry curvature dipole in the monolayer topological insulator WTe_2. *Nat. Phys.* **14**, 900–906 (2018).
6. Zhang, Y., van den Brink, J., Felser, C. & Yan, B. Electrically tuneable nonlinear anomalous Hall effect in two-dimensional transition-metal dichalcogenides WTe_2 and $MoTe_2$. *2D Mater.* **5**, 044001 (2018).
7. You, J.-S., Fang, S., Xu, S.-Y., Kaxiras, E. & Low, T. Berry curvature dipole current in the transition metal dichalcogenides family. *Phys. Rev. B* **98**, 121109 (2018).
8. Shi, L.-K & Song, J. C. W. Symmetry, spin-texture, and tunable quantum geometry in a WTe_2 monolayer. *Phys. Rev. B* **99**, 035403 (2019).
9. Ma, Q. et al. Observation of the nonlinear Hall effect under time-reversal-symmetric conditions. *Nature* **565**, 337–342 (2019).
10. Kang, K., Li, T., Sohn, E., Shan, J. & Mak, K. F. Nonlinear anomalous Hall effect in few-layer WTe_2. *Nat. Mater.* **18**, 324–328 (2019).
11. Du, Z. Z., Wang, C. M., Lu, H.-Z. & Xie, X. C. Band signatures for strong nonlinear Hall effect in Bilayer WTe_2. *Phys. Rev. Lett.* **121**, 266601 (2018).
12. Qian, X., Liu, J., Fu, L. & Li, J. Quantum spin Hall effect in two-dimensional transition metal dichalcogenides. *Science* **346**, 1344–1347 (2014).
13. Tang, S. et al. Quantum spin Hall state in monolayer 1T′-WTe_2. *Nat. Phys.* **13**, 683–687 (2017).
14. Fei, Z. et al. Edge conduction in monolayer WTe_2. *Nat. Phys.* **13**, 677–682 (2017).
15. Wu, S. et al. Observation of the quantum spin Hall effect up to 100 kelvin in a monolayer crystal. *Science* **359**, 76 (2018).
16. Sajadi, E. et al. Gate-induced superconductivity in a monolayer topological insulator. *Science* **362**, 922–925 (2018).
17. Fatemi, V. et al. Electrically tunable low-density superconductivity in a monolayer topological insulator. *Science* **362**, 926–929 (2018).
18. Soluyanov, A. A. et al. Type-II Weyl semimetals. *Nature* **527**, 495–498 (2015).
19. Ali, M. N. et al. Large, non-saturating magnetoresistance in WTe_2. *Nature* **514**, 205–208 (2014).
20. Sie, E. J. et al. An ultrafast symmetry switch in a Weyl semimetal. *Nature* **565**, 61–66 (2019).
21. Fei, Z. et al. Ferroelectric switching of a two-dimensional metal. *Nature* **560**, 336 (2018).
22. Anderson, P. W. & Blount, E. I. Symmetry considerations on martensitic transformations: "Ferroelectric" metals? *Phys. Rev. Lett.* **14**, 217–219 (1965).
23. Wang, H. & Qian, X. Ferroicity-driven nonlinear photocurrent switching in time-reversal invariant ferroic materials. *Sci. Adv.* **5**, eaav9743 (2019).
24. Li, R. et al. Weyl ferroelectric semimetal. *Preprint at arXiv:1610.07142* (2016).
25. Weng, H., Fang, C., Fang, Z., Bernevig, B. A. & Dai, X. Weyl semimetal phase in noncentrosymmetric transition-metal monophosphides. *Phys. Rev. X* **5**, 011029 (2015).
26. Sipe, J. E. & Shkrebtii, A. I. Second-order optical response in semiconductors. *Phys. Rev. B* **61**, 5337–5352 (2000).

27. Tsirkin, S. S., Puente, P. A. & Souza, I. Gyrotropic effects in trigonal tellurium studied from first principles. *Phys. Rev. B* **97**, 035158 (2018).
28. Morimoto, T., Zhong, S., Orenstein, J. & Moore, J. E. Semiclassical theory of nonlinear magneto-optical responses with applications to topological Dirac/Weyl semimetals. *Phys. Rev. B* **94**, 245121 (2016).
29. Rostami, H. & Polini, M. Nonlinear anomalous photocurrents in Weyl semimetals. *Phys. Rev. B* **97**, 195151 (2018).
30. Hohenberg, P. & Kohn, W. Inhomogeneous electron gas. *Phys. Rev. B* **136**, B864–B871 (1964).
31. Kohn, W. & Sham, L. J. Self-consistent equations including exchange and correlation effects. *Phys. Rev.* **140**, A1133–A1138 (1965).
32. Kresse, G. & Furthmüller, J. Efficient iterative schemes for *ab initio* total-energy calculations using a plane-wave basis set. *Phys. Rev. B* **54**, 11169–11186 (1996).
33. Marzari, N., Mostofi, A. A., Yates, J. R., Souza, I. & Vanderbilt, D. Maximally localized Wannier functions: theory and applications. *Rev. Mod. Phys.* **84**, 1419–1475 (2012).
34. Qian, X. et al. Quasiatomic orbitals for *ab initio* tight-binding analysis. *Phys. Rev. B* **78**, 245112 (2008).
35. Du, Z. Z., Wang, C. M., Li, S., Lu, H.-Z. & Xie, X. C. Disorder-induced nonlinear Hall effect with time-reversal symmetry. *Nat. Commun.* **10**, 3047 (2019).
36. Isobe, H., Xu, S.-Y. & Fu, L. High-frequency rectification via chiral electrons in nonlinear crystals. *Preprint at arXiv:1812.08162* (2018).
37. Nagaosa, N., Sinova, J., Onoda, S., MacDonald, A. H. & Ong, N. P. Anomalous Hall effect. *Rev. Mod. Phys.* **82**, 1539–1592 (2010).
38. Bouhon, A., Slager, R.-J. & Bzdušek, T. Non-abelian reciprocal braiding of Weyl Nodes. *Preprint at arXiv:1907.10611* (2019).
39. Blöchl, P. E. Projector augmented-wave method. *Phys. Rev. B* **50**, 17953–17979 (1994).
40. Perdew, J. P., Burke, K. & Ernzerhof, M. Generalized gradient approximation made simple. *Phys. Rev. Lett.* **77**, 3865–3868 (1996).
41. Klimeš, J., Bowler, D. R. & Michaelides, A. Chemical accuracy for the van der Waals density functional. *J. Phys. Condens. Matter* **22**, 022201 (2010).
42. Krukau, A. V., Vydrov, O. A., Izmaylov, A. F. & Scuseria, G. E. Influence of the exchange screening parameter on the performance of screened hybrid functionals. *J. Chem. Phys.* **125**, 224106 (2006).
43. Mostofi, A. A. et al. An updated version of wannier90: a tool for obtaining maximally-localised Wannier functions. *Comput. Phys. Commun.* **185**, 2309–2310 (2014).

ACKNOWLEDGEMENTS

This work was supported by the National Science Foundation (NSF) under award number DMR-1753054. Portions of this research were conducted with the advanced computing resources provided by Texas A&M High Performance Research Computing.

AUTHOR CONTRIBUTIONS

X.Q. conceived the project. H.W. and X.Q. developed first-principles tight-binding approach for computing nonlinear susceptibility tensor. H.W. performed the calculations. Both H.W. and X.Q. analyzed the results and wrote the manuscript.

COMPETING INTERESTS

The authors declare no competing interests.

ADDITIONAL INFORMATION

Supplementary information is available for this paper at https://doi.org/10.1038/s41524-019-0257-1.

Correspondence and requests for materials should be addressed to X.Q.

Reprints and permission information is available at http://www.nature.com/reprints

Publisher's note Springer Nature remains neutral with regard to jurisdictional claims in published maps and institutional affiliations.